Materials Advances

ROYAL SOCIETY OF CHEMISTRY

PAPER

View Article Online
View Journal | View Issue

Cite this: *Mater. Adv.*, 2022, 3, 658

Water-assisted synthesis of lead-free Cu based fluorescent halide perovskite nanostructures†

Hari Shankar, Abha Jha and Prasenjit Kar *

Received 14th September 2021,
Accepted 1st November 2021

DOI: 10.1039/d1ma00849h

rsc.li/materials-advances

Lead halide perovskite nanocrystals (NCs) are eminent for their emission properties, but lead (Pb) toxicity and moisture instability have become an impediment to their commercial use. To resolve these obstacles and develop an environmentally friendly energy material at a low cost, we discuss the synthesis of lead-free Cs_2CuCl_4, Cs_2CuBr_4, and $Cs_2CuBr_2Cl_2$ perovskite nanostructures with non-toxic copper (Cu). In this work, we adopted a ligand assisted re-precipitation (LARP) synthesis route for material preparation at room temperature. Water is used as a polar solvent to dissolve the metal halide precursors rapidly. For the first time, we achieved a high PLQY of 38% in mixed halide perovskite $Cs_2CuBr_2Cl_2$NCs with blue luminescence in an aqueous medium. Cu-based perovskites Cs_2CuCl_4, Cs_2CuBr_4, and $Cs_2CuBr_2Cl_2$ demonstrated their morphology as square nanoplates, nanorods, and rectangular nanoplates, respectively. The long-term photoluminescence stability of these stored perovskites was also examined at different intervals for 45 days.

1. Introduction

For the last few years, lead halide perovskites have been well known in the perovskite territory as energy materials for optoelectronic applications such as in light-emitting diodes (LEDs), lasers, and photodetectors.[1–4] These applications are due to their unique properties such as high photoluminescence quantum yields (PLQY), narrow emission bands, and band gap flexible tunability.[5–7] However, the instability and toxicity of lead inhibit their utilization in materials.[8] The skeleton of lead halide perovskites becomes damaged in contact with moisture, air, heat, light, and polar solvents.[9–12] Recently, people have made systematic efforts to eliminate toxicity in perovskites to substitute lead with other elements.

Recently, lead has been replaced by elements such as tin (Sn), bismuth (Bi), antimony (Sb), germanium (Ge), copper (Cu), and zinc (Zn).[13–18] Among them, Cu ions have been used as alternatives to develop high efficiency with low toxicity, cost-effective, and stable lead-free perovskites.[17] Cu is an essential metal ion for the animal body. It is a base chunk of many proteins and enzymes. These prodigious functions exhibited by Cu ion make it environmentally friendly.[19] Generally, Pb forms a 3D perovskite structure. Apart from this, Cu generates a 2D system because Cu has small ionic radii compared to Pb.[20] The general formula of Cu-based 2D perovskites is A_2CuX_4, where A is a monovalent cation (ammonium, Cs^+) and X is a halide ion (Cl^-, Br^- and I^-).

Zhou and coworkers have reported (p-F-$C_6H_5C_2H_4$–$NH_3)_2CuBr_4$ and $(CH_3(CH_2)_3NH_3)_2CuBr_4$, 2D perovskites with power conversion efficiencies (PCEs) of 0.51% and 0.63%, respectively.[21] Cortecchia *et al.* synthesized $MA_2CuCl_xBr_{4-x}$ hybrid 2D perovskites and reported their optical absorption and emission properties.[22] Elsemanet *et al.* developed Cu-based $(CH_3NH_3)_2CuX_4$, $[(CH_3NH_3)_2CuCl_4$, $(CH_3NH_3)_2CuCl_2I_2$, and $(CH_3NH_3)_2CuCl_2Br_2]$ perovskites and observed their absorbance and photoluminescence features.[23]

Recently, Yang *et al.* generated Cs_2CuCl_4, Cs_2CuBr_4, and $Cs_2Cu(Br/I)_4$ blue–green luminescent perovskite quantum dots by using *N*,*N*-dimethylformamide (DMF) and dimethylsulfoxide (DMSO) polar solvents to dissolve a precursor with *n*-octylamine and oleic acid as capping ligands in *n*-octane non-polar solvent adopting a ligand assisted re-precipitation (LARP) method at room temperature. Noteworthily, the solubility of CsBr and CsCl in polar solvents (DMF and DMSO) is low compared to that of $CuCl_2$ and $CuBr_2$ precursors.[24] To overcome this solubility concern and check the long-term stability of lead-free halide perovskites, an ideal amount of water can dissolve the halide precursors in the LARP method.

Inspired by the above approach, here, we have synthesized Cu-based Cs_2CuCl_4, Cs_2CuBr_4, and $Cs_2CuBr_2Cl_2$ perovskite nanocrystals by using the LARP approach at room temperature as shown in Fig. 1. In this strategy, we dissolved metal halide precursors in water and injected them into oleylamine and oleic acid, containing isopropanol solvent with constant stirring.

Department of Chemistry, Indian Institute of Technology Roorkee, Uttarakhand-247667, India. E-mail: kar.prasen@gmail.com, prasenjit.kar@cy.iitr.ac.in

† Electronic supplementary information (ESI) available. See DOI: 10.1039/d1ma00849h

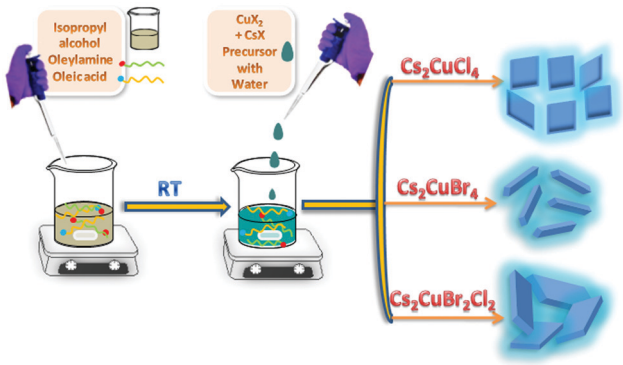

Fig. 1 Schematic illustration of the water-assisted synthesis of blue fluorescent Cs_2CuCl_4 square nanoplates, Cs_2CuBr_4 nanorods, and $Cs_2CuBr_2Cl_2$ rectangular nanoplates.

The obtained NCs show blue fluorescence under UV light and displayed square-shaped nanoplate, nanorod, and rectangular nanoplate morphology for Cs_2CuCl_4, Cs_2CuBr_4, and $Cs_2CuBr_2Cl_2$, respectively.

2. Experimental

2.1 Chemicals

All the chemicals and solvents were used without further purification. Cesium chloride (99.99%), cesium bromide (99.99%), copper(II) bromide (99%), and oleylamine (70%) were purchased from Sigma Aldrich. Copper(II) chloride (95%) was purchased from Himedia, and isopropanol (99.5%) and oleic acid were obtained from SRL.

2.2 Synthesis of Cs_2CuCl_4

In a typical preparation, 0.2 mmol of $CuCl_2$ and 0.4 mmol of CsCl were dissolved in 0.5 mL double distilled water and a light pale blue colored precursor solution was obtained. In the meantime, another solution was prepared by adding 50 μL oleylamine and 100 μL oleic acid in 3 mL isopropanol with vigorous stirring. After that, the water precursor solution was injected into the oleylamine and oleic acid-containing isopropanol solution and this mixed solution was stirred for 1 h at room temperature. Eventually, we found a dark cyan-colored solution. Later, 500 μL of the colloidal solution was dispersed into 2 mL of isopropanol solvent. The product was purified and isolated by centrifugation at 7000 rpm for 3 min. After discarding the precipitate it was used for subsequent characterization.

2.3 Synthesis of Cs_2CuBr_4

0.2 mmol of $CuBr_2$ and 0.4 mmol of CsBr were dissolved in 0.5 mL double distilled water and a dark pale blue colored precursor solution was obtained. In the meantime, another solution was prepared by adding 50 μL oleylamine and 100 μL oleic acid in 3 mL isopropanol with vigorous stirring. After that, the water precursor solution was injected into the oleylamine and oleic acid-containing isopropanol solution and this mixed solution was stirred for 1 h at room temperature. Eventually, we found a dark cyan-colored solution. Later, 500 μL of the colloidal solution was dispersed into 2 mL of isopropanol solvent. The product was purified and isolated by centrifugation at 7000 rpm for 3 min. After discarding the precipitate it was used for subsequent characterizations.

2.4 Synthesis of $Cs_2CuBr_2Cl_2$

The mixed bromide chloride perovskite $Cs_2CuBr_2Cl_2$, was synthesized by dissolving 0.2 mmol of $CuBr_2$ and 0.4 mmol of CsCl in 0.5 mL double distilled water and a pale blue colored precursor solution was obtained. In the meantime, another solution was prepared by adding 50 μL oleylamine and 100 μL oleic acid in 3 mL isopropanol with vigorous stirring. After that, the water precursor solution was injected into the oleylamine and oleic acid-containing isopropanol solution and this mixed solution was stirred for 1 h at room temperature. Eventually, we found a dark cyan-colored solution. Later, 500 μL of the colloidal solution was dispersed into 2 mL of isopropanol solvent. The product was purified and isolated by centrifugation at 7000 rpm for 3 min. After discarding the precipitate it was used for subsequent characterization.

2.5 Characterization

A Shimadzu UV-vis 2450 spectrophotometer was used for recording the UV-vis absorption spectra in the range of 290–565 nm. Photoluminescence spectra were obtained by using a Horiba Scientific Fluoromax-4C spectrophotometer. A quartz cuvette of 10 mm path length and 3 mL volume was used for collecting the spectra. Time-correlated single-photon counting (TCSPC) studies and fluorescence lifetime decay measurements were recorded using a 1 cm quartz cell on a Horiba Jobin Yvon, equipped with a picosecond diode laser (model Pico Brite-375L and DD-450L) as the excitation source. Quantum yield as an absolute quantum yield was measured directly by using an Edinburgh instruments FLS 980. We have prepared a highly diluted solution of NCs and measured the absolute quantum yield. Powder XRD was carried out on a Bruker-D8 using Cu-Ka radiation with an accelerating voltage of 40 kV from 10 to 60° with a rate of 1° min^{-1}. The thin film samples were prepared on silica glass. Field emission scanning electron microscopy (FESEM) images were recorded for all the samples using a Carl Zeiss Ultra Plus. The thin film samples were prepared on silica glass. Transmission electron microscopy (TEM) studies were carried out on a TEM TECHNAI G2 20 S-TWIN. These were performed by taking a drop of highly diluted sample on a carbon-coated copper grid. Fourier transform infrared spectroscopy (FTIR) spectra of all the samples were recorded by using a Thermo Scientific Nicolet 6700. The spectral subtraction provided reliable and reproducible results. X-ray photoelectron spectroscopy (XPS) analysis of the thin films of perovskites prepared on silica glass was carried out on an XPS instrument with model no. PHI 5000 Versa Probe III for surface analysis. Thermogravimetric analysis (TGA) measurement was carried out by using a TA instruments EXSTAR TG/DTA 6300. The samples were heated from room temperature to 1000 °C at a rate of 10 °C min^{-1}, under a nitrogen flux of 200 mL min^{-1}.

3. Results and discussion

The optical properties of Cs_2CuCl_4, Cs_2CuBr_4, and $Cs_2CuBr_2Cl_2$ were investigated using absorption and emission spectra (Fig. 2).

The absorption properties of all the samples were recorded by using UV-visible ranges. Fig. 2a exhibits absorption onset, centered at 364.94 nm, which is associated with excitonic absorption.[25,26] Along with this, the band gap of all the samples was measured by using the direct band gap Tauc prescription in Fig. S1a–c(ESI†), which shows a 3.06 eV band gap for Cs_2CuCl_4, 3.03 eV for Cs_2CuBr_4, and 3.05 eV for $Cs_2CuBr_2Cl_2$, respectively. The emission studies of the blue luminescent samples were investigated through photoluminescence (PL) spectra at an excitation wavelength of 350 nm. The as-prepared samples show the emission band at 434 nm in Fig. 2b. The emission band is unaffected in all the samples, suggesting that the emission is not the intrinsic band emission but due to some extrinsic character. This extrinsic character arises due to the presence of defect states or surface states. The PL intensities characterize the existence of defect states. Larger particles have higher luminescence intensities.

This contrasts with the nanoparticle properties, which suggest that the surface to volume ratio is inversely proportional to the particle size and hence the luminescence.

One explanation is that the luminescence is due to defects associated with the core or volume of the nanoparticle and not on the surface.[24,27]

The un-shifted emission spectra of Cs_2CuCl_4, Cs_2CuBr_4, and $Cs_2CuBr_2Cl_2$ perovskites can be due to d–d transitions in the d levels for Cu. This phenomenon has been described in a previous report, where varying the halide ions in $(CH_3NH_3)_2CuCl_4$, $(CH_3NH_3)_2CuCl_2I_2$, and $(CH_3NH_3)_2CuCl_2Br_2$ perovskites didn't cause the emission wavelength to shift.[23] In another report, the photoluminescence spectra exhibited the same emission band for MA_2CuCl_4, $MA_2CuCl_2Br_2$, $MA_2CuClBr_3$, and $MA_2CuCl_{0.5}Br_{3.5}$ perovskites.[22]

The time-resolved PL curves of all the samples were recorded at λ_{max} = 435 nm with the excitation wavelength of 350 nm (Fig. 2c). The decay was fitted to three-exponential curves representing average lifetimes of 4.53 ns, 3.78 ns, and 3.64 ns for $Cs_2CuBr_2Cl_2$, Cs_2CuCl_4, and Cs_2CuBr_4 respectively (details in Table S1, ESI†). The decrease in PL lifetime is due to the decrease in the particle size of NCs as proposed in previous reports.[28] For larger NCs, the excitation binding energy is reduced.[29] The photoluminescence excitation (PLE) spectra of Cs_2CuCl_4, Cs_2CuBr_4, and $Cs_2CuBr_2Cl_2$ were recorded with the peak at 378 nm as shown in Fig. 2d–f.

The absolute PLQYs of all the samples were observed using a fluorescence spectrometer at an excitation wavelength of 350 nm. The PLQYs of all the samples were determined to be 31.52%, 25.14%, and 38.23% for Cs_2CuCl_4, Cs_2CuBr_4, and $Cs_2CuBr_2Cl_2$ respectively. The high PLQY in hybrid perovskite $Cs_2CuBr_2Cl_2$ may lead to an improvement in the radiative recombination rate.[30]

The phase of the synthesized Cs_2CuCl_4, Cs_2CuBr_4, and $Cs_2CuBr_2Cl_2$ perovskites was identified by using X-ray diffraction (XRD) analysis, as shown in Fig. 3a. The diffraction pattern with peaks at 2θ = 16.64°, 19.57°, 20.66°, 21.74°, 22.81°, 23.35°, 23.67°, 24.52°, 26.32°, 27.47°, 28.41°, 28.78°, 29.14°, 30.25°, 30.71°, 30.88°, 32.52°, 33.22°, 33.51°, 35.19°, 36.42°, 36.81°, 36.95°, 37.08°, 38.02°, 39.59°, 39.72°, 40.22°, and 40.85° and even further, corresponding to diffractions from the (120), (210), (121), (201), (211), (220), (002), (031), (112), (022), (310), (040),

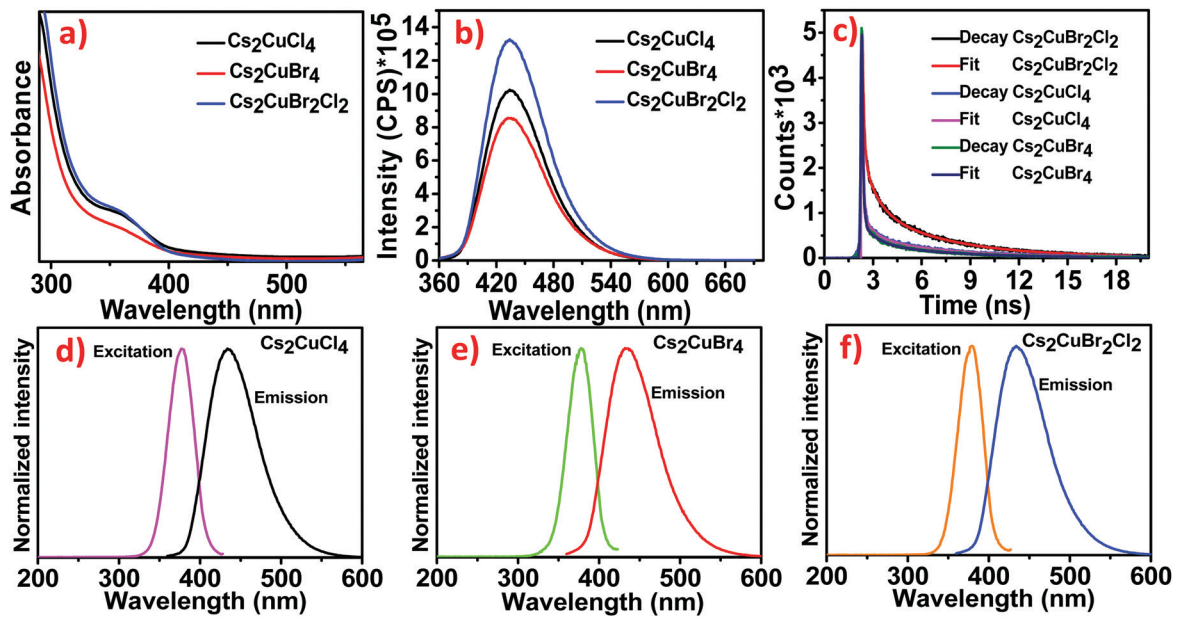

Fig. 2 (a) UV-Visible spectra of Cs_2CuCl_4, Cs_2CuBr_4 and $Cs_2CuBr_2Cl_2$. (b) PL spectral studies of Cs_2CuCl_4, Cs_2CuBr_4 and $Cs_2CuBr_2Cl_2$. (c) PL time decay studies of Cs_2CuCl_4, Cs_2CuBr_4 and $Cs_2CuBr_2Cl_2$ perovskites. (d–f) Excitation and emission spectra of the as-prepared Cs_2CuCl_4, Cs_2CuBr_4 and $Cs_2CuBr_2Cl_2$ perovskite NCs.

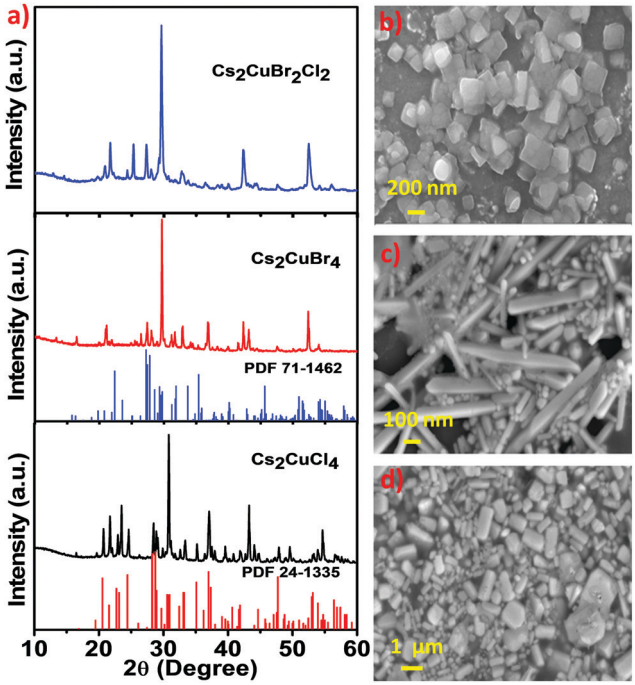

Fig. 3 (a) X-ray diffraction pattern of Cs_2CuCl_4, Cs_2CuBr_4 and $Cs_2CuBr_2Cl_2$. (b–d) SEM images of Cs_2CuCl_4, Cs_2CuBr_4 and $Cs_2CuBr_2Cl_2$ present square shaped nanoplates, nanorods and rectangular shaped nanoplates, respectively.

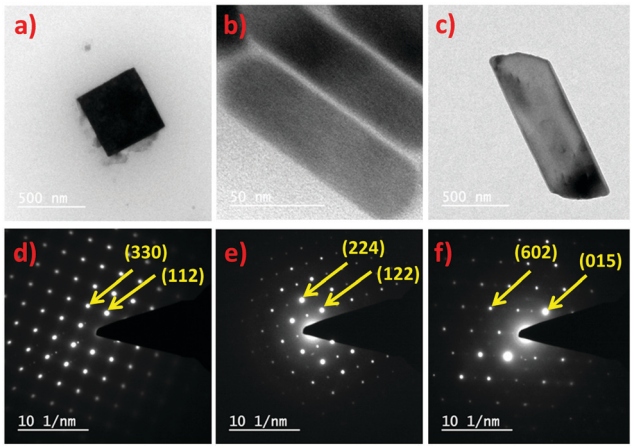

Fig. 4 (a) TEM image of square-shaped nanoplates of Cs_2CuCl_4 at 500 nm scale bar. (b) TEM image of Cs_2CuBr_4 nanorods at 50 nm scale bar. (c) TEM image of rectangular-shaped nanoplates of $Cs_2CuBr_2Cl_2$ at 500 nm scale bar. (d) SAED pattern of Cs_2CuCl_4 nanoplates. (e) SAED pattern of Cs_2CuBr_4 nanorods. (f) SAED pattern of $Cs_2CuBr_2Cl_2$ nanoplates.

(202), (140), (212), (320), (141), (222), (321), (330), (241), (400), (312), (042), (051), (420), (203), (340), and (213) planes of the orthorhombic Cs_2CuCl_4 perovskite is consonant with the standard (PDF #24-1335).[31] In Fig. 3a, the diffraction pattern of Cs_2CuBr_4 peaks at 16.23°, 19.92°, 20.89°, 21.84°, 24.99°, 25.39°, 26.28°, 27.21°, 27.98°, 28.94°, 29.42°, 31.18°, 31.70°, 33.97°, 34.48°, 35.41°, 36.51°, 36.86°, 37.42°, 38.28°, 38.80°, and 40.03° and even further, corresponding to (102), (112), (210), (211), (121), (113), (022), (203), (122), (104), (213), (114), (123), (303), (031), (321), (015), (124), (322), (230), (321), and (224) faces indicates the orthorhombic phase and is consonant with the standard (PDF #71-1462).[31] In this sequence, the XRD pattern of $Cs_2CuBr_2Cl_2$ shows similarity with the diffraction patterns of Cs_2CuCl_4 and Cs_2CuBr_4. Consequently, the mixed halide perovskite $Cs_2CuBr_2Cl_2$ also exhibits an orthorhombic crystal structure. However, the minor impurity peaks in these diffraction patterns are related to cesium and copper halides. Avoiding these minor impurities from the samples is very difficult as observed in previous reports.[31,32] We used water as a solvent during the material synthesis which may be a cause of unknown diffraction peaks.[33]

The morphological structure of all three perovskites was observed by using scanning electron microscopy (SEM). Fig. 3b shows the square-shaped nanoplate morphology of Cs_2CuCl_4, the nanorod morphology of Cs_2CuBr_4 is shown in Fig. 3c, and the obtained mixed halide perovskite $Cs_2CuBr_2Cl_2$ exhibited rectangular-shaped nanoplates, as shown in Fig. 3d. The composition of the elements in these perovskites was detected by energy-dispersive X-ray spectroscopy (EDS). Fig. S2a, ESI,† shows the existence of Cs, Cu, and Cl elements, which indicate the formation of Cs_2CuCl_4. The presence of Cs, Cu, and Br in Fig. S2b, ESI† indicates the constitution of Cs_2CuBr_4 and the elemental constituents Cs, Cu, Br, and Cl in Fig. S2c, ESI† provide the composition of $Cs_2CuBr_2Cl_2$ perovskite.

The morphology of all three perovskites was demonstrated further by transmission electron microscopy (TEM), which corroborates the SEM analysis. The obtained Cs_2CuCl_4 shows a square nanoplate shape of ~8.25 nm thickness with an edge length of 402 nm (Fig. 4a). The selected area electron diffraction (SAED) pattern in Fig. 4d indicates its crystalline nature. In this image, the measured crystal planes (112) and (330) are consistent with the XRD pattern. Interestingly, the TEM image in Fig. 4b indicates the emergence of the nanorod morphology of Cs_2CuBr_4 perovskite. The diameter and length of rods were estimated to be ~35 nm and 118 nm, respectively. Fig. 4e highlights the crystalline SAED pattern of Cs_2CuBr_4 nanorods with (122) and (224) planes identical to the orthorhombic phase as related to X-ray diffraction. The TEM image of the mixed halide perovskite $Cs_2CuBr_2Cl_2$, as shown in Fig. 4c, presents a rectangular nanoplate shape with a thickness of ~21.17 nm and 1030 nm edge length.

The SAED pattern of the crystalline rectangular nanoplates (Fig. 4f) has characteristic crystal planes of (015) and (602) for orthorhombic crystal structures as observed in the XRD pattern of $Cs_2CuBr_2Cl_2$.

Fourier Transform Infrared (FTIR) spectroscopy was performed to decode the interaction between the perovskite crystal surface and organic ligands. Generally, this technique is used to identify the vibration modes of ligands. As shown in Fig. S3, ESI,† FTIR spectral positions have emerged to be almost similar for all as-prepared perovskite nanostructures, indicating the cooperation of perovskites with the same organic surface type ligands (OLA and OA). The peak at 1460 cm^{-1} was assigned to the symmetric stretching vibration mode in $-COO^-$ of oleic acid, and the peak at around 1633 cm^{-1} indicates the N–H scissor bending vibration of the $-NH_2$ group in oleylamine. The peak at around 1719 cm^{-1}

is ascribed to the asymmetric starching vibration in $-COO^-$ of oleic acid. A broad vibration peak appears at about 3421 cm^{-1} which is a clear indication of the presence of water in the obtained product. The peaks are centered at 2861 cm^{-1} and 2925 cm^{-1} due to the C–H bond stretching vibration of $-CH_3$ and $-CH_2$ in the aliphatic hydrocarbon chain.

The presence of constituent elements Cs, Cu, Br, and Cl in all three perovskites has been confirmed by using X-ray photoelectron spectroscopy (XPS) studies. In Fig. S4a, ESI,† the XPS survey scan for Cs_2CuCl_4 presents the characteristic binding energies of Cs, Cu, and Cl at appropriate positions. Moreover, in the narrow scans for Cs 3d, Cu 2p and Cl 2p as shown in Fig. S4b–d, ESI,† the corresponding binding energies of the Cs $3d_{3/2}$, Cs $3d_{5/2}$, Cu $2p_{1/2}$, Cu $2p_{3/2}$, Cl $2p_{1/2}$, and Cl $2p_{3/2}$ orbitals are centered at 737.92, 724.01, 953.80, 933.75, 199.96, and 198.92 eV, respectively. These critical energy data indicate the formation of Cs_2CuCl_4 perovskite. The binding energy of Cs $3d_{3/2}$ and Cs $3d_{5/2}$ emerged at 737.85 and 723.85, respectively (Fig. S5b, ESI†). The peaks in Fig. S5c and d, ESI† at 953.68, 934.06, 71.53, 69.11, and 62.92 eV correspond to Cu $2p_{1/2}$, Cu $2p_{3/2}$, Br $3d_{1/2}$, Br $3d_{3/2}$, and Br $3d_{5/2}$, respectively, which indicate the successful synthesis of Cs_2CuBr_4. The appearance of binding energy peaks of Cs $3d_{3/2}$, Cs $3d_{5/2}$, Cu $2p_{1/2}$, Cu $2p_{3/2}$, Br $3d_{1/2}$, Br $3d_{3/2}$, Br $3d_{5/2}$, Cl $2p_{1/2}$, and Cl $2p_{3/2}$ at 737.96, 724.01, 953.97, 934.12, 71.60, 69.18, 62.78, 199.65 and, 198.95 eV respectively, demonstrates the formation of mixed halide perovskite $Cs_2CuBr_2Cl_2$ (Fig. S6a–e, ESI†).

The time-dependent photoluminescence stability of Cs_2CuCl_4, Cs_2CuBr_4, and $Cs_2CuBr_2Cl_2$ perovskite nanostructures was also recorded for 45 days under ambient conditions. As shown in Fig. 5a–c, the PL intensity for all these compounds decreased gradually in the prolonged time interval. Moreover, after 45 days, Cs_2CuCl_4, $Cs_2CuBr_2Cl_2$, and Cs_2CuBr_4 exhibited reasonably high PL intensity in the presence of water. These studies indicate the long-term stability of lead-free perovskite nanostructures in aqueous medium.

The photostability tests of Cs_2CuCl_4, Cs_2CuBr_4, and $Cs_2CuBr_2Cl_2$ perovskite nanocrystals were performed under continuous UV light (365 nm) irradiation for 200 h as shown in Fig. 5d–f. A significant reduction in emission intensity was observed after UV light irradiation which may lead to the formation of new traps. It is noteworthy that the blue emission was still shown in all the samples after 200 h under high energy continuous UV light (365 nm) irradiation which confirms that these perovskites are reasonably photostable.

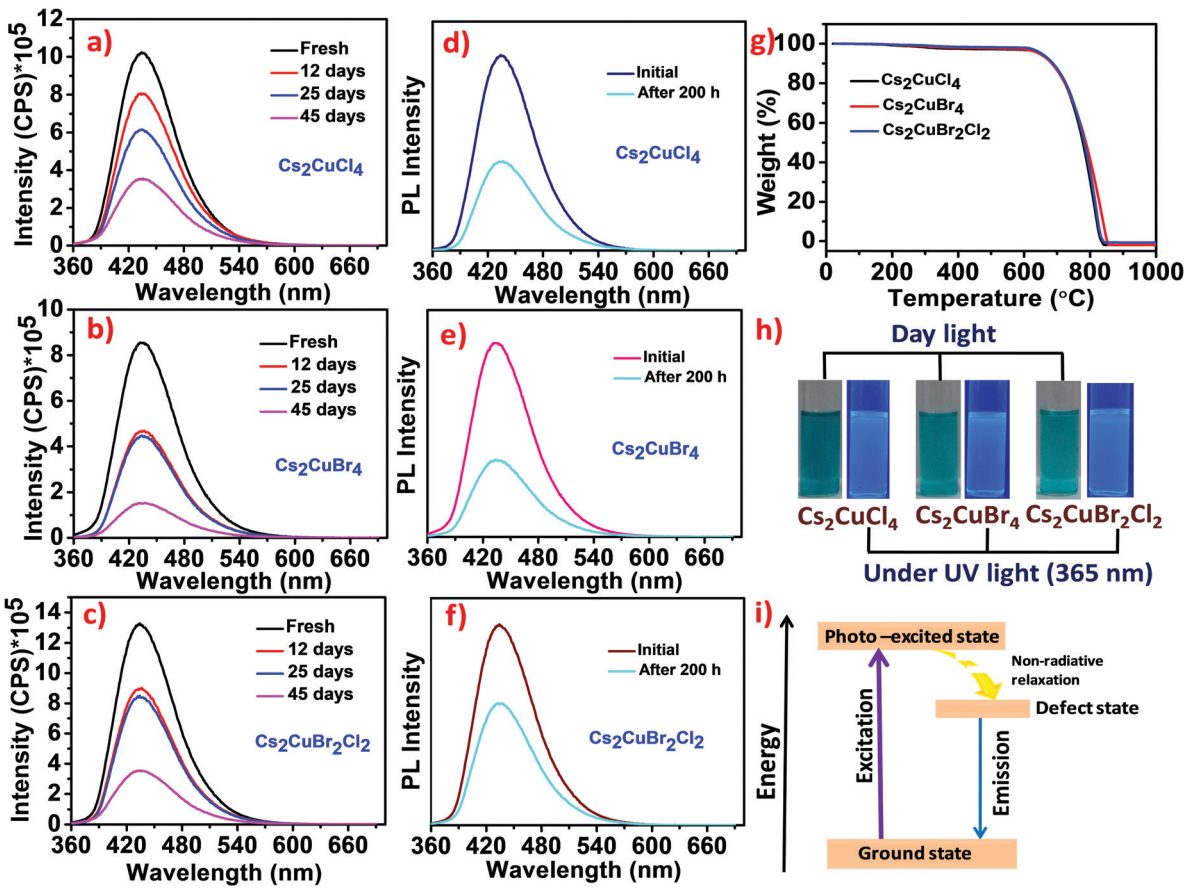

Fig. 5 (a–c) Time-dependent PL studies of Cs_2CuCl_4, Cs_2CuBr_4, and $Cs_2CuBr_2Cl_2$ perovskite NCs respectively. (d–f) The PL spectra of Cs_2CuCl_4, Cs_2CuBr_4, and $Cs_2CuBr_2Cl_2$ perovskite NCs under continuous UV light (365 nm) irradiation for 200 h. (g) Thermograms of Cs_2CuCl_4, Cs_2CuBr_4, and $Cs_2CuBr_2Cl_2$ perovskites. (h) Photographs of Cs_2CuCl_4, Cs_2CuBr_4 and $Cs_2CuBr_2Cl_2$ perovskite samples under daylight and UV light (365 nm). (i) Schematic model representing the emission mechanism.

The thermal stability of these perovskites was investigated by using thermogravimetric analysis (TGA) studies. As shown in Fig. 5g, the thermograms of Cs_2CuCl_4, Cs_2CuBr_4, and $Cs_2CuBr_2Cl_2$ perovskites are similar in nature. In the first step, a minor weight loss of about 1.4% was observed between 80–191 °C due to the evaporation of isopropanol and water molecules from the perovskites.[5] The second small weight loss of around 2–4% between 200–374 °C indicates the deduction of oleylamine and oleic acid from the surface of perovskites.[34] Significant weight loss was observed at around 606 °C, which represents the degradation of the perovskite framework. Cahen and co-workers have reported the thermal degradation of $CsPbBr_3$ NCs at around 580 °C.[35] Compared to these results, lead-free Cu-based halide perovskites exhibit higher thermal stability than lead halide perovskites. In Fig. 5h, photographs of the Cs_2CuCl_4, Cs_2CuBr_4, and $Cs_2CuBr_2Cl_2$ perovskite samples show blue luminescence under UV light (365 nm).

There are several types of emission mechanisms that have been explained in previous reports about Cu-based luminescent materials.[36] Chen and their group have demonstrated that Cu^+ plays an important role in the blue emission of $Rb_8CuSc_3Cl_{18}$ and $Rb_8CuY_3Cl_{18}$.[33] Another report described the emission due to the generation of the $CuCl_4$ complex in $CuAlCl_4$.[37] On the other hand, Xu *et al.* achieved emission in non-emissive ZnO nanorods on Cu^{2+} doping where Cu defects were observed as the cause of the emission band.[38] In this context, Davis and co-workers suggested that the formation of Cu^{2+} defects could be responsible for the emission in Cs_2CuCl_4 nanoparticles.[39]

In our report, the emission in Cs_2CuCl_4, Cs_2CuBr_4, and $Cs_2CuBr_2Cl_2$ can arise due to the formation of intraband defects (Cu(II) defects) in nanomaterials.[39] The emission mechanism can be demonstrated through a schematic energy level model as shown in Fig. 5i. Upon excitation, electrons transfer from the ground state to the photo-excited state followed by relaxation in the defect state which in turn comes back to the ground state in a radiative pathway exhibiting a broad band of blue emission.

4. Conclusions

In summary, we successfully synthesized Cu-based Cs_2CuCl_4, Cs_2CuBr_4, and $Cs_2CuBr_2C_{l2}$ perovskite nanostructures at room temperature by using water solvent. We observed a higher PLQY in the mixed halide perovskite $Cs_2CuBr_2Cl_2$ compared with Cs_2CuCl_4 and Cs_2CuBr_4. The obtained compounds displayed high thermal stability and exhibited fluorescence over 45 days under ambient conditions. In this strategy, the synthesis of lead-free halide perovskite NCs in the aqueous medium suggests an alternative route towards environmentally friendly and environmentally stable materials for the perovskite community, hence considering their toxicity and instability. This step has become essential for their commercialization in the future. It can be expected that these studies on transition metal halide perovskites will provide a realistic platform for the next generation of perovskites in optoelectronic device materials.

Conflicts of interest

The authors declare no conflicts of interest.

Acknowledgements

This work was supported by the Indian Institute of Technology Roorkee. P. K. gratefully acknowledges the Science and Engineering Research Board (CRG/2020/000702), New Delhi, India, for financial support. The authors acknowledge the Institute Instrumentation Centre (IIC), IIT Roorkee, for the instrument facility. H. S. acknowledges UGC, India, for a doctoral research fellowship. A. J. acknowledges MHRD, India, for a junior research fellowship.

Notes and references

1 W. Zou, R. Li, S. Zhang, Y. Liu, N. Wang, Y. Cao, Y. Miao, M. Xu, Q. Guo, D. Di, L. Zhang, C. Yi, F. Gao, R. H. Friend, J. Wang and W. Huang, *Nat. Commun.*, 2018, **9**, 608.
2 J. Xing, Y. Zhao, M. Askerka, L. N. Quan, X. Gong, W. Zhao, J. Zhao, H. Tan, G. Long, L. Gao, Z. Yang, O. Voznyy, J. Tang, Z.-H. Lu, Q. Xiong and E. H. Sargent, *Nat. Commun.*, 2018, **9**, 3541.
3 P. Bansal and P. Kar, *Chem. Commun.*, 2019, **55**, 6543–6546.
4 C. H. Kang, I. Dursun, G. Liu, L. Sinatra, X. Sun, M. Kong, J. Pan, P. Maity, E.-N. Ooi, T. K. Ng, O. F. Mohammed, O. M. Bakr and B. S. Ooi, *Light: Sci. Appl.*, 2019, **8**, 94.
5 X. Zhang, X. Bai, H. Wu, X. Zhang, C. Sun, Y. Zhang, W. Zhang, W. Zheng, W. W. Yu and A. L. Rogach, *Angew. Chem., Int. Ed.*, 2018, **57**, 3337–3342.
6 Q. A. Akkerman, V. D'Innocenzo, S. Accornero, A. Scarpellini, A. Petrozza, M. Prato and L. Manna, *J. Am. Chem. Soc.*, 2015, **137**, 10276–10281.
7 L. Protesescu, S. Yakumin, M. I. Bodnarchuk, F. Krieg, R. Caputo, C. H. Hendon, R. X. Yang, A. Walsh and M. V. Kovalenko, *Nano Lett.*, 2015, **15**, 3692–3696.
8 S. Yang, Y. Wang, P. Liu, Y.-B. Cheng, H. J. Zhao and H. G. Yang, *Nat. Energy*, 2016, **1**, 15016.
9 H. Shankar, P. Bansal, W. W. Yu and P. Kar, *Chem. – Eur. J.*, 2020, **26**, 12242–12248.
10 S. Zou, Y. Liu, J. Li, C. Liu, R. Feng, F. Jiang, Y. Li, J. Song, H. Zeng, M. Hong and X. Chen, *J. Am. Chem. Soc.*, 2017, **139**, 11443–11450.
11 P. Bansal, Y. Khan, G. K. Nim and P. Kar, *Chem. Commun.*, 2018, **54**, 3508–3511.
12 X. Li, F. Cao, D. Yu, J. Chen, Z. Sun, Y. Shen, Y. Zhu, L. Wang, Y. Wei, Y. Wu and H. Zeng, *Small*, 2017, **13**, 1603996.
13 T. C. Jellicoe, J. M. Richter, H. F. J. Glass, M. Tabachnyk, R. Brady, S. E. Dutton, A. Rao, R. H. Friend, D. Credgington, N. C. Greenham and M. L. Böhm, *J. Am. Chem. Soc.*, 2016, **138**, 2941–2944.
14 M. Leng, Y. Yang, K. Zeng, Z. Chen, Z. Tan, S. Li, J. Li, B. Xu, D. Li, M. Hautzinger, Y. Fu, T. Zhai, L. Xu, G. Niu, S. Jin and J. Tang, *Adv. Funct. Mater.*, 2018, **28**, 1704446.

15 J. Zhang, Y. Yang, H. Deng, U. Farooq, X. Yang, J. Khan, J. Tang and H. Song, *ACS Nano*, 2017, **11**, 9294–9302.
16 P. Cheng, T. Wu, J. Zhang, Y. Li, J. Liu, L. Jiang, X. Mao, R.-F. Lu, W.-Q. Deng and K. Han, *J. Phys. Chem. Lett.*, 2017, **8**, 4402–4406.
17 R. Valiente and F. Rodríguez, *ACS Appl. Mater. Interfaces*, 2020, **12**, 37807–37810.
18 H. Shankar, S. Ghosh and P. Kar, *J. Alloys Compd.*, 2020, **844**, 156148.
19 J. S. Lewis, R. Laforest, T. L. Buettner, S.-K. Song, Y. Fujibayashi, J. M. Connett and M. J. Welch, *Proc. Natl. Acad. Sci. U. S. A.*, 2001, **98**, 1206–1211.
20 L. Liang and P. Gao, *Adv. Sci.*, 2018, **5**, 1700331.
21 X.-P. Cui, K.-J. Jiang, J.-H. Huang, Q.-Q. Zhang, M. J. Su, L.-M. Yang, Y.-L. Song and X. Q. Zhou, *Synth. Met.*, 2015, **209**, 247–250.
22 D. Cortecchia, H. A. Dewi, J. Yin, A. Bruno, S. Chen, T. Baikie, P. P. Boix, M. Grätzel, S. Mhaisalkar, C. Soci and N. Mathews, *Inorg. Chem.*, 2016, **55**, 1044–1052.
23 A. M. Elseman, A. E. Shalan, S. Sajid, M. M. Rashad, A. M. Hassan and M. Li, *ACS Appl. Mater. Interfaces*, 2018, **10**, 11699–11707.
24 J. T. Griffiths, F. W. R. Rivarola, N. J. L. K. Davis, R. Ahumada-Lazo, J. A. Alanis, P. Parkinson, D. J. Binks, W. Y. Fu, F. D. L. Pena, M. B. Price, A. Howkins, I. Boyd, C. J. Humphreys, N. C. Greenham and C. Ducati, *ACS Appl. Energy Mater.*, 2019, **2**, 6998–7004.
25 B. Guo, C. Luo, C. Yan, B. Sun, W. Li and W. Yang, *J. Phys. Chem. C*, 2020, **124**, 26076–26082.
26 Y. Lekina and Z. X. Shen, *J. Sci.: Adv. Mater. Devices*, 2019, **4**, 189–200.
27 D. Bozyigit, W. M. M. Lin, N. Yazdani, O. Yarema and V. Wood, *Nat. Commun.*, 2015, **6**, 6180.
28 V. Malgras, S. Tominaka, J. W. Ryan, J. Henzie, T. Takei, K. Ohara and Y. Yamauchi, *J. Am. Chem. Soc.*, 2016, **138**, 13874–13881.
29 Y. Tong, F. Ehrat, W. Vanderlinden, C.-C. Daw, J. K. Stolarczyk, L. Polavarapu and A. S. Urban, *ACS Nano*, 2016, **10**, 10936–10944.
30 G. Jin, D. Zhang, P. Pang, Z. Ye, T. Liu, G. Xing, J. Chen and D. Ma, *J. Mater. Chem. C*, 2021, **9**, 916–924.
31 P. Yang, G. Liu, B. Liu, X. Liu, Y. Lou, J. Chen and Y. Zhao, *Chem. Commun.*, 2018, **54**, 11638–11641.
32 Y. Ren and S. Lü, *Chem. Eng. J.*, 2021, **417**, 129223.
33 J. Lin, H. Chen, J. Kang, L. N. Quan, Z. Lin, Q. Kong, M. Lai, S. Yu, L. Wang, L.-W. Wang, M. F. Toney and P. Yang, *Matter*, 2019, **1**, 180–191.
34 H. Yang, Y. Zhang, J. Pan, J. Yin, O. M. Bakr and O. F. Mohammed, *Chem. Mater.*, 2017, **29**, 8978–8982.
35 M. Kulbak, S. Gupta, N. Kedem, I. Levine, T. Bendikov, G. Hodes and D. Cahen, *J. Phys. Chem. Lett.*, 2016, **7**, 167–172.
36 Q. Ge, R. Zheng, J. Lin and H. Chen, *Mater. Lett.*, 2020, **277**, 128280.
37 M. Sullivan and J. D. Martin, *J. Am. Chem. Soc.*, 1999, **121**, 10092–10097.
38 C. X. Xu, X. W. Sun, X. H. Zhang, L. Ke and S. J. Chua, *Nanotechnology*, 2004, **15**, 856–861.
39 E. P. Booker, J. T. Griffiths, L. Eyre, C. Ducati, N. C. Greenhamand and N. J. L. K. Davis, *J. Phys. Chem. C*, 2019, **123**, 16951–16956.